Article:

eprints@whiterose.ac.uk
https://eprints.whiterose.ac.uk/

Design of adjustable Tuned Mass Dampers using elastomeric O-rings

N. Tang[a,*], J.A. Rongong, N.D. Sims

[a]*Department of Mechanical Engineering, The University of Sheffield, Sheffield, S1 3JD, UK.*

Abstract

Tuned mass dampers (TMDs) are widely used in passive vibration control, and have been implemented on many engineering structures. In general, the design of TMDs is unique to each application; the choice of damping material and its in-situ performance are key issues that can affect design and prototyping costs. The present contribution demonstrates that TMDs can be built using ubiquitous and low-cost elastomeric O-rings. It is shown that the damping and stiffness characteristics of the O-ring can be predicted a priori, in order to achieve an initial design that is fit for purpose. Furthermore, it is shown that the nonlinear characteristics of the O-ring enable the device to be easily tuned in-situ, in order to optimise the final system. Finally, the simple configuration of the device makes it well suited to through-mounting or surface-mounting on thin-walled flexible structures such as beams and plates.

Keywords: variable stiffness, elastomeric damping, vibration control, analytical model, experimental study

1. Introduction

Polymeric materials are frequently used as the energy dissipating element in vibration control strategies as they are reliable and inexpensive. Elastomeric anti-vibration mounts are widely used for isolation while free and constrained layer dampers are highly effective for flexible plates and shells. These classic damping technologies are less effective for structures where the dynamic strains, in comparison to the vibration level, are very low or are localised to inaccessible regions. One possible solution for vibration mitigation in these conditions is the Tuned Mass Damper(TMD).

A TMD, first described publicly by Den Hartog [1], is a damped oscillator that is attached to a vibrating structure. The vibration energy of the primary structure is then transferred to this secondary oscillator or dissipated by the incorporated damping. Passive TMDs are always attractive as they are easy to use, low cost and reliable. However, they suffer from a narrow working frequency band and can usually only target one single resonance. Many studies have been carried out to improve the performance of the conventional TMD [2, 3] and recently there has been growing interest techniques where the moving mass in the secondary oscillator is replaced by either an inerter [4, 5] or part of the host structure itself (non-conventional TMD [6] which causes a reduction of the overall system mass. One approach that aims to address wider working frequencies is to incorporate variable stiffness TMDs [7, 8] but these devices suffer from high additional weight. Other approaches have included the development of semi-active or active control strategies [9–12] what have resulted in TMDs that suppress multi-mode vibration. However, use of these devices is limited because of the additional volume and complex circuitry involved.

Simple yet adjustable TMDs can be constructed if the spring and damper elements are formed by one or more O-rings made from elastomers such as nitrile or natural rubber. Modification of the stiffness can by achieved by altering the axial deformation of an O-ring. Energy dissipation occurs as the elastomer is subjected to dynamic strains and is dominated by relaxation and recovery processes that occur within and between the long chain molecules that form the material [13]. Consequently, in order to design an

---

effective O-ring TMD, it is necessary to be able to predict the stiffness and damping properties of the O-ring itself. For elastomeric O-rings, Lindley [14] derived the load-deflection relationship in the tensile-compressive direction. However, there has been limited research to establish analytical models for O-rings, subjected to transverse shear or rocking. This becomes important when the O-ring is used in a TMD configuration, because for simple designs there is no mechanical constraint to inhibit off-axis motion.

This paper develops a design procedure for elastomeric O-ring TMDs, considering how the stiffness can be tuned in-situ. Then, the influence of multi-degree-of-freedom behaviour (tension-compression and rocking) is evaluated, because this could be detrimental or advantageous for vibration control of practical flexible structures. Section 2 begins by illustrating the proposed TMD design, and using Finite Element Analysis (FEA) to illustrate its behaviour. Section 3 presents experimental analysis of O-rings to demonstrate their dynamic stiffness and damping characteristics. The influence of static compression is considered in order to explore whether in-situ TMD tuning is possible. Section 4 develops an analytical model of the O-ring performance that could be used for device design purposes. This is then validated against experimental data in Section 5. Section 6 then demonstrates a practical application of the approach on an engineering structure, exploring MDOF effects and demonstrating the tuning capabilities. Section 7 briefly considers additional design considerations for practical applications while Section 8 draws some conclusions.

2. Configuration and initial evaluations of TMD incorporating O-rings

The configuration of the proposed adjustable O-ring TMD is shown in Figure 1. This damper uses two identical circular discs and elastomeric O-rings that are mechanically attached to host structure. Two threaded holes are made in the middle of these discs. The two halves of the TMD are clamped onto the host structure using a threaded rod that passes through the host structure without touching it. The static compression of the O-rings can be adjusted using the threaded rod resulting in a simple device that minimises interface friction. In this design therefore, the O-rings not only provide the stiffness and damping for the system, they isolate the threaded rod, which serves as part of the TMD mass. Consequently, there are no redundant components in the design. Furthermore, the circular cross-section of the O-ring means that static compression applied using the threaded rod is expected to influence the O-ring stiffness. Thus, if the stiffness and damping can be predicted, then the designer is able to follow a very simple methodology, namely:

1. selection of the threaded rod and attached discs based on the desired TMD mass;
2. choice of O-ring material, diameter, and wire diameter (i.e. diameter of the O-ring's solid section), in order to achieve desired damping and stiffness;
3. final adjustment of the static compression to optimise the resonance frequencies.

Before developing this methodology, the behaviour of an example device is explored using FEA. The dimensions of the device are given in Table 1.

2.1. Numerical model

An initial numerical study was conducted in order to identify the vibration modes typically occurring in such devices. The analysis first needed to obtain the deformed condition caused by the static pre-load, which in practice, is always required in order to hold the damper to the host structure. To minimise computational effort, the deformed shape for the O-ring cross-section was first obtained using a 2D axisymmetric finite strain analysis using a high density mesh. This deformed shape was then used to construct a 3D model from which natural frequencies and mode shapes were calculated. In this model, the threaded rod was simplified to a cylinder for the sake of computational effort. This cylinder was bonded to the mass block to ensure the boundary condition between threaded rod and discs remain unchanged. Friction between the O-ring and discs was ignored for the modal analysis. Most of this FE model was made from solid 20-noded quadratic hexahedron elements. Since one of the key design features for this kind of TMD is stiffness of the O-rings, a fine meshing strategy was required for the O-rings. In total, the model involved 6190 elements, of which approximately two thirds were used to mesh the O-rings themselves.
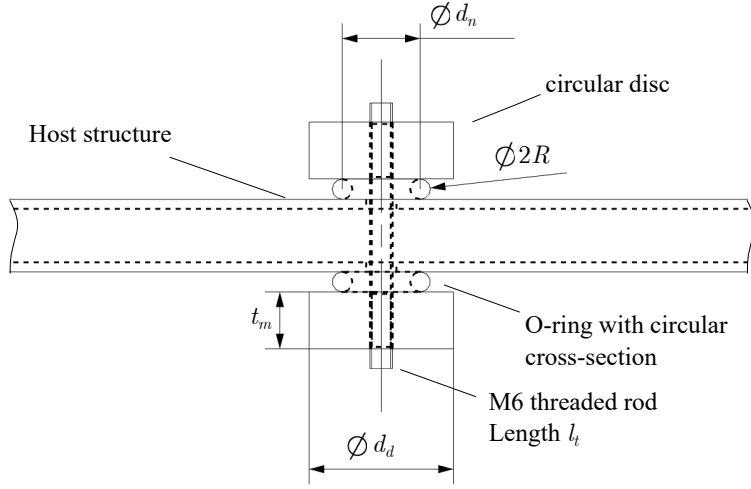
Figure 1: Adjustable TMD using elastomer O-ring

Table 1: Additional properties of the adjustable TMD

Components	Variables	Value
Disc	Dimensions $- \phi d_d \times t_m$	ϕ 38.1 mm $\times$ 15 mm
	Mass $- m_d$	152 g
	Young's modulus $- E_d$	117 GPa
O-ring	Mass $- m_O$	1.8 g
	Type	BS312
	Elastic modulus $- E$	9.3 MPa
	Poisson's ratio $- \nu$	0.49
	Nominal diameter $- d_n$	20.57 mm
	wire diameter $- 2R$	5.33 mm
Threaded rod	Dimensions	M6 $\times$ 1
	Length $- l_t$	70 mm
	Mass $- m_t$	9 g
	Young's modulus $- E_t$	230 GPa

2.2. Working modes

Excluding twisting motion, this device displays three types of vibration mode: compression, rocking and shear. Typical mode shapes are shown in Figure 2. It should be noted that at higher frequencies, many of the modes involve local resonance within the O-rings which makes estimating stiffness difficult. These modes are neglected in the present study.
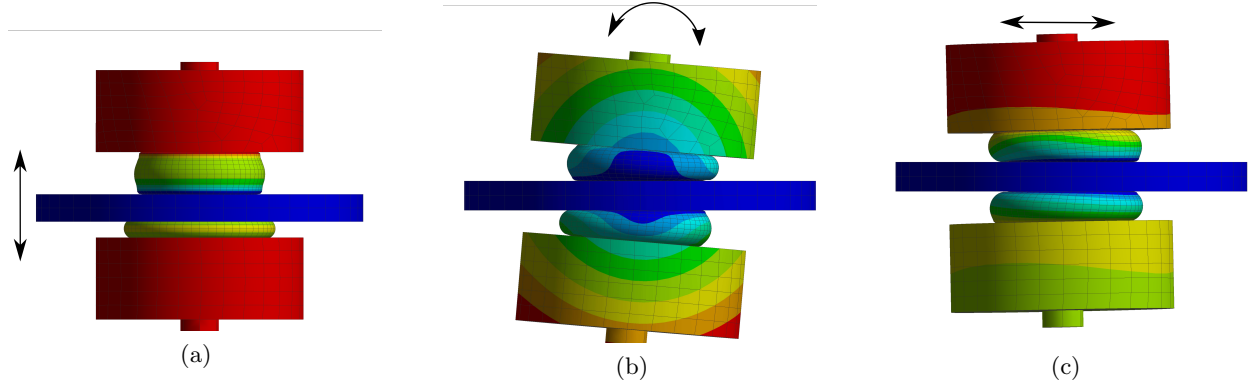

Figure 2: Working modes of the O-ring TMD (a) compression mode (b) rocking mode (c) shear mode.

The compression mode (Fig 2a) corresponds to the simplest intended design of the device, but the other modes may have an unintended influence on the host structure, which could be detrimental or beneficial. For example, transverse vibrations of the host structure will excite two damper modes (compression - Fig 2a - and rocking - Fig 2b), that can interact with the motion of the host structure. This is in contrast to an ideal TMD. However, the additional mode could give desirable performance depending on the mode shapes of the host structure.

When this system is subjected to static compression, the natural frequencies move to higher frequencies. To demonstrate this behaviour, a comparison between two different static compressions applied to the O-ring was carried out.

Table 2: Comparison of resonance frequencies for different modes(results obtained using Ansys and verified using Abaqus)

Static compression	Compression mode	Rocking mode	Shear mode
0.05 mm	274 Hz	113 Hz	121 Hz
2.1 mm	639 Hz	413 Hz	256 Hz
Frequency ratio $\omega_{2.1}\omega_{0.05}^{-1}$	2.12	3.66	2.33

It can be seen from Table 2 that the resonance frequencies of this damper increase considerably with static compression. The sensitivity of the stiffness to the geometric nonlinearity in different directions can be seen in the differences by which the natural frequencies increase. The higher sensitivity of the rocking mode to initial compression occurs because this deformation not only increases the contact area, it also moves material further from the centreline of the damper increasing its resistance to transverse rotation. For other modes, the position with regard to the damper centreline is not important. Therefore, a greater stiffening can be observed for rocking modes.

To conclude, the working frequencies of these devices are sensitive to static compression showing that the O-ring condition is fundamentally important to this type of TMD. Although multi-direction vibration suppression can potentially be achieved, as motion exists parallel and perpendicular to the damper axis, this is not the focus of this paper. Instead, this work considers the use of the compression and rocking modes that couple with transverse vibration of the host structure.

3. Experimental evaluations of compressive stiffness and damping of O-rings

The dynamic response of an elastomeric element is normally affected by both geometric and material properties. A suitable model therefore, should be able to account for changes in either property. Material properties for elastomers are usually represented using hyperelastic-viscoelastic models while the geometric changes are estimated analytically or using finite element analysis. This section describes work carried out to obtain test data on O-rings for use in model validation studies. Axial stiffness and damping are obtained under various excitation frequencies, static preloads and dynamic displacement amplitudes. All work was carried out at room temperature.

3.1. Damping of various elastomers

The damping level within a TMD is an important design criterion - simply increasing this damping level does not result in an improved damper. Often, the best performance for a TMD is achieved when the internal damping ratio is around 0.1 [15]. For this TMD therefore, efforts were made to find commercial O-rings made from polymers having operating-range loss factors around 0.2.

Comparisons were made between O-rings made from different materials using low strain, low frequency, axial compression tests. The equipment used was a Metravib VA2000 visco-analyser, which was capable of applying steady and sinusoidal loading with a nominal peak value of 100 N. The test machine allowed monitoring of the load through a built-in piezoelectric force sensor, and the motion via a linear variable differential transformer.

The test involved placing an O-ring between parallel loading plates on the test machine, applying a 0.3 mm static compression and then a 2.5 Hz sinusoidal load with a nominal amplitude of 0.025 mm. Each O-ring studied was made from a synthetic elastomer with a nominal hardness of 70 IRHD. All materials considered were operating in the rubbery zone, far from the glass transition temperature, hence significant temperature and frequency dependence was considered unlikely. Softening was noticeable during the first few loading cycles, which was attributed to the Mullins effect [16], so cycling was continued until the hysteresis loops stabilised.

The details for these O-rings and measured energy loss factors are shown in Table 3.

Table 3: Loss factors of candidate O-ring materials

Type	Material	Energy loss factor
Poly 70	Polyurethane	0.23
BR 70	Butyl	0.32
ACM 70	Polyacrylate	0.46
NBR 70	Nitrile	0.20

As a material with relatively low cost and damping was considered desirable for this application, the nitrile O-rings were selected for use in this work.

3.2. Dynamic compressive stiffness of elastomeric O-rings

Dynamic compressive tests using a uni-axial, servo-hydraulic test machine (MTS 858 tabletop system) were carried out to obtain O-ring load-deflection data in the axial direction at more realistic loading levels. The system was operated in displacement-controlled mode using motion of the upper grip. A 25 kN capacity load cell attached between the lower grip and the load frame provided force measurements.

Tests were carried out at three different excitation frequencies – 2.5 Hz, 10 Hz and 30 Hz – and nine different compression levels. The nitrile O-rings had a nominal diameter of 20.57 mm and a wire diameter of 5.33 mm. At each test condition, the O-ring was subjected to 50 cycles of displacement-controlled sinusoidal loading with a peak-to-peak amplitude of 0.5 mm. The hysteresis loop was obtained using the ensemble average of the force trace. From this, the stiffness and energy loss were found. A third order Butterworth low-pass filter with a cut-off frequency of 50 Hz was used to remove noise from experimental data.
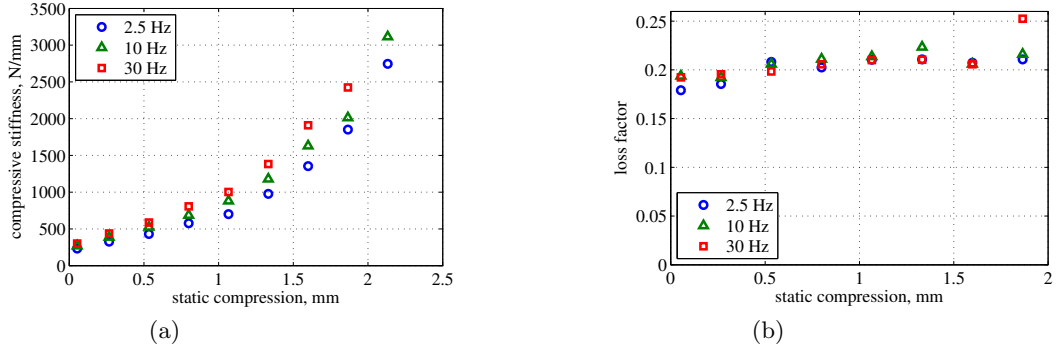
Figure 3: Effect of static compression and excitation frequencies for O-rings (a) stiffness behaviour (b) damping behaviour

Figure 3 shows that the stiffness increases dramatically with axial compression while the loss factor remains almost unchanged. The primary factor affecting stiffness is the cross-sectional geometry which changes under load. Bending and elastic buckling of molecular chains dominates the elasticity of a polymer in the low-strain region. At high compressions, densification of molecule chains may also cause further stiffening, also referred to material nonlinearity. The slight increase in stiffness with excitation frequency can be attributed to viscoelasticity.

For the condition where the static compression was 0.85 mm and the excitation frequency was 2.5 Hz, the testing was carried out at different dynamic displacement amplitudes. Dynamic displacement dependent stiffness and damping are presented in Figure 4.
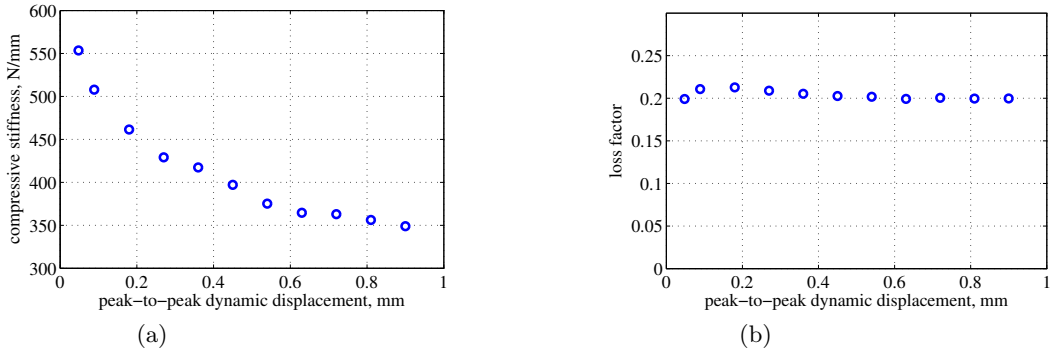

Figure 4: Effect of peak-to-peak displacement amplitude on (a) axial stiffness and (b) loss factor

It can be seen from Figure 4 that damping does not change significantly for different dynamic amplitudes. The stiffness, however, drops considerably as the dynamic amplitude increases. This phenomenon is thought to be an example of the Payne effect of rubber materials [17] in which the modulus of a reinforced elastomeric material reduces reversibly as the strain amplitude is increased, due to the re-organisation of weak physical bonds in the microstructure.

Figure 5 illustrates the typical normalised hysteresis loops when subjected to different levels of dynamic excitations. At low amplitude, the hysteresis loop traces and ellipse - as would be expected from a linear viscoelastic material. At high dynamic amplitude, the shape of the loop reveals significant underlying nonlinearity - the source of which could be geometric effects, Payne's effect or interfacial friction between the O-ring and restricting plates. Comparisons of Figures 3 and 4 shows that sensitivity of the stiffness to static compression is much more significant than that seen from dynamic loading. Consequently, the dynamic amplitude might be important in the final application but it need not influence the initial design and sizing of the TMD.
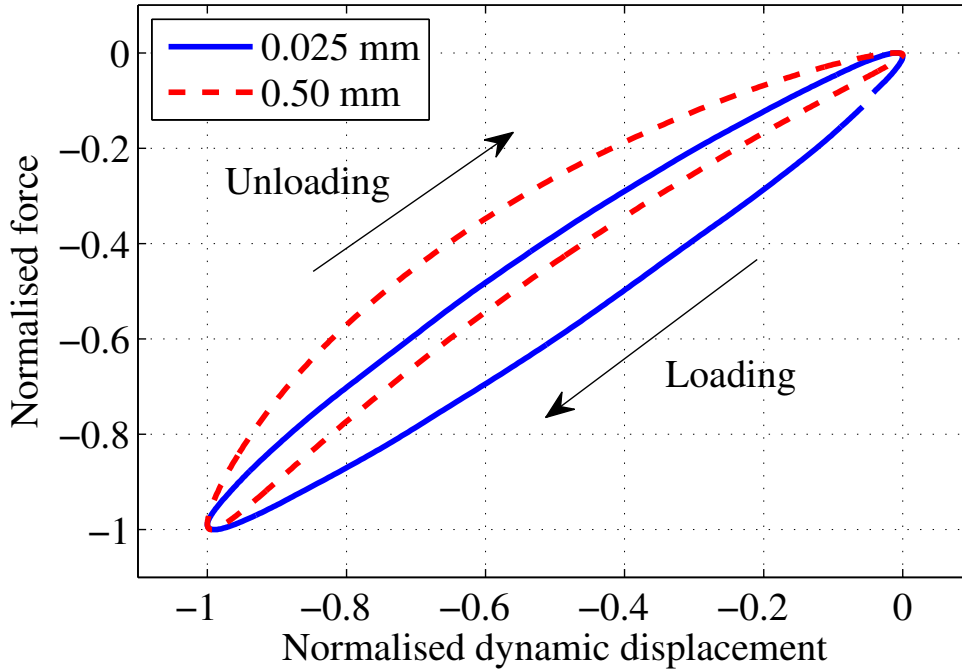
Figure 5: Typical normalised hysteresis loops when subjected to different dynamic displacement amplitudes

3.3. Summary

To summarise, nitrile O-rings have been observed to provide attractive properties for the proposed TMD. An obvious deformation-dependent stiffness can be observed, which provides a sound basis for designing an adjustable TMD. Also, the damping remains almost unchanged. This provides an opportunity for widening the working frequency range of this TMD. However, in order to achieve the simple design methodology described in Section 2, it is important that the O-ring stiffness can be easily predicted. This will be addressed in the next section.

4. Analytical model of elastomeric O-rings

To develop a simple analytical model of the O-ring stiffness, the following assumptions were made:

- The elastomer is assumed isotropic and homogeneous, displaying nonlinear elasticity.

- The mechanical model developed for the O-rings is deformation-dependent only. The effect of the excitation frequencies and the temperature is explained by the elastic modulus.

- The damping is assumed linear viscous, when subject to a particular frequency.

- The plane strain model is used, and therefore, no strain in the directions perpendicular to the selected cross section is considered.

- A rectangular ring with deformed height and contact length is used to represent the load-carrying of O-ring at given compressions. The shape of the free edges of the deformed cross-section can be represented using a parabolic function [18].

- Friction between the O-ring and restricting plates is ignored.

4.1. Tensile-compressive behaviour

First, the analytical model in the tensile-compressive direction is developed, as this model forms the basis for those in other directions. The coordinates and notation used in this analytic model subject to tensile-compressive motion is shown in Figure 6. The analytical nonlinear stiffness model, comprising k_g and k_h, is
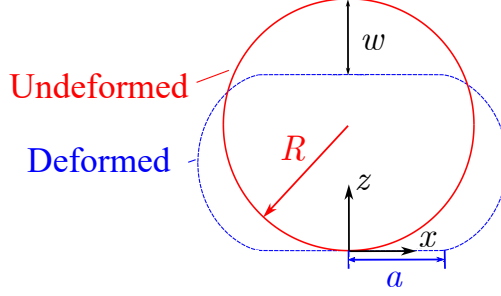

Figure 6: Coordinates and notations of the analytical model for O-ring in compression

then considered for this elastomeric O-ring. In this analytical model, k_g accounts for the stiffening caused by cross-sectional local expansion, while k_h explains the expansion of the nominal diameter of the O-ring, especially when subjected to high static compressions. As the O-ring is axisymmetric, a plane strain model incorporating geometric nonlinearity through the cross-section is applied to establish the load-deflection relationship.

When an axial compression is applied to an O-ring, its cross-section changes. This phenomenon of local expansion can be represented by the Hertz contact method and, as shown by George [19] the pressure distribution in the axial direction is approximately elliptical. Following Johnson's derivations [20], the stress at any point along the centreline of the cross-section inside the O-ring is given by

$$\sigma_x = \frac{P}{d_n \pi^2} \left[\frac{1}{R} - \frac{2(a^2 + 2z^2)}{a^2(a^2 + z^2)^{1/2}} + \frac{4z}{a^2} \right] \tag{1}$$

$$\sigma_z = \frac{P}{d_n \pi^2} \left[\frac{1}{R} - \frac{2}{(a^2 + z^2)^{1/2}} - \frac{2}{2R - z} \right] \tag{2}$$

where d_n is the nominal diameter of the O-ring. σ_x and σ_z are stress distribution in the radial and axial directions respectively. z is the distance from the loading surface of the O-ring cross section, P is the applied load and R is cross-sectional radius. a is half contact length shown in Figure 6 and can be given by,

$$a = \sqrt{\frac{4PR(1 - \nu^2)}{d_n \pi^2 E}} \tag{3}$$

in which ν is Poisson's ratio, E is the elastic modulus and is a function of temperature and excitation frequencies. Using the classic strain-stress relationship, the axial strain at any point is,

$$\epsilon_z = \frac{1 - \nu^2}{E} \left[\sigma_z - \left(\frac{\nu}{1 - \nu} \right) \sigma_x \right] \tag{4}$$

Following this, the axial deformation of the O-ring at its centre can be represented as,

$$w = 2 \int_0^R \epsilon_z \mathrm{d}z \tag{5}$$

The deformation of O-ring can be obtained by substituting Equation 1 to 4 into Equation 5,

$$w = \frac{2(1 - v^2)}{E} \frac{P}{d_n \pi^2} \left[\frac{1 - 2\nu}{1 - \nu} - \frac{2(1 - 2\nu)}{1 - \nu} A_1 - \frac{4\nu}{(1 - \nu) a^2} A_2 + 2 \ln 2 + A_3 \right] \tag{6}$$

where A_1 refers to,

$$\ln\left(R + \sqrt{a^2 + R^2}\right) - \ln(a) \tag{7}$$

A_2 is given by,

$$\frac{1}{2}R(a^2 + R^2)^{1/2} - \frac{1}{2}a^2 \ln\left[(a^2 + R^2)^{1/2} + R\right] + \frac{1}{2}a^2 \ln(a) \tag{8}$$

and A_3 is,

$$\frac{2\nu R^2}{a^2(1 - \nu)} \tag{9}$$

The deflection-load relationship for a O-ring can be obtained by substituting Equation 3 into Equation 6. Taking the differential of this relation, the nonlinear stiffness from geometric variation with compression is given by,

$$k_g = \left(\frac{\partial w}{\partial P}\right)^{-1} \tag{10}$$

Testing reported in the previous section shows that the O-ring stiffens considerably with compression level (refer to Figure 3). The developed model is not able to match this behaviour completely when the material modulus is assumed linear. One reason for this difference is that the model may not represent accurately the radial expansion of the O-ring itself. The other possible reason is the re-arrangement of the crosslinks in the molecular chains of the polymer. A polynomial expression that allows for the stiffening of the O-ring at large deformation, was introduced by Lindley [14]. This expression was based on test data from a number of different O-rings and is given as,

$$k_h = 600\pi r_n E\left(\frac{w}{2R}\right)^5 \tag{11}$$

The semi-empirical model stiffness is then defined as the sum of the geometrical stiffness and polynomial terms such that,

$$k_c = k_g + k_h \tag{12}$$

Figure 7 shows the comparison of analytical and experimental results. Note that two experimental data points exist for one static compression level. The upper one is obtained from the gradient of the load-deflection curve during the loading operation while the lower one is during unloading. Both models work well when the static compression is less than 0.8 mm (i.e. 15% of the wire diameter) for the device tested. When the static compression is higher than 0.8 mm, the developed model under-estimates the compressive stiffness whereas the semi-empirical model reaches acceptable accuracy. The limitation of the semi-empirical model is that the polynomial terms do not relate directly to measurable properties: they were identified originally by Lindley for natural rubber specimens and have been shown here to be appropriate for nitrile rubber. There is no guarantee though that the same polynomial terms are appropriate for a polymer with significantly different large-strain load-deflection behaviour. However in this work, as the low strain behaviour of the two models is identical, the semi-empirical model was used for subsequent analyses.

It can also be seen from Figure 7 that the axial stiffness is slightly different between analytical and experimental results. This small difference in the stiffness might come from the estimation errors for the elastic modulus of rubber.

Energy dissipation for this TMD mainly comes from material damping within the elastomer and hence, damping from interfacial friction is ignored. The loss factor for the O-ring can be estimated using the ratio of dissipated and storage strain energy. Limited research has been carried out on the effect of high steady strain on the energy dissipation and particularly, the loss factor, of a polymer. Assuming that linear viscoelasticity – the damping is independent of strain – applied in this case, the loss factor of this given elastomer can represent that of O-ring directly. The analytical damping model of the O-ring is presented in Figure 8.

Figure 8 shows that the single damping value used for the analytical model is close to the experimental results, especially when the static compression is moderate.
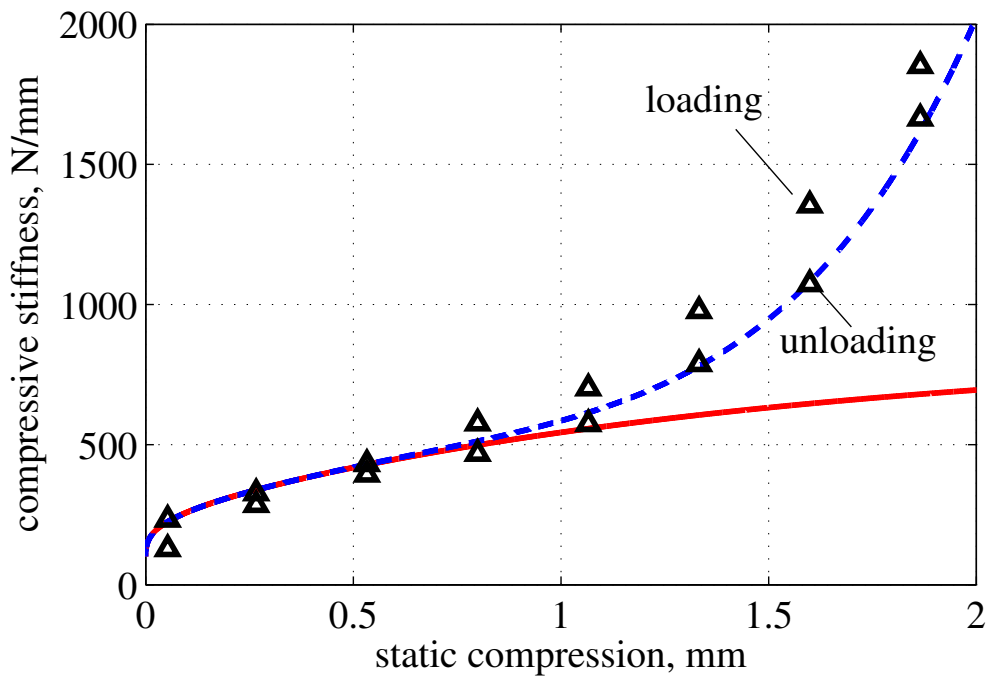
Figure 7: Analytical stiffness model for O-ring. Red solid line refers to developed model (k_g). Blue dash line refers to semi-empirical model (k_c). Black triangles refer to experimental data
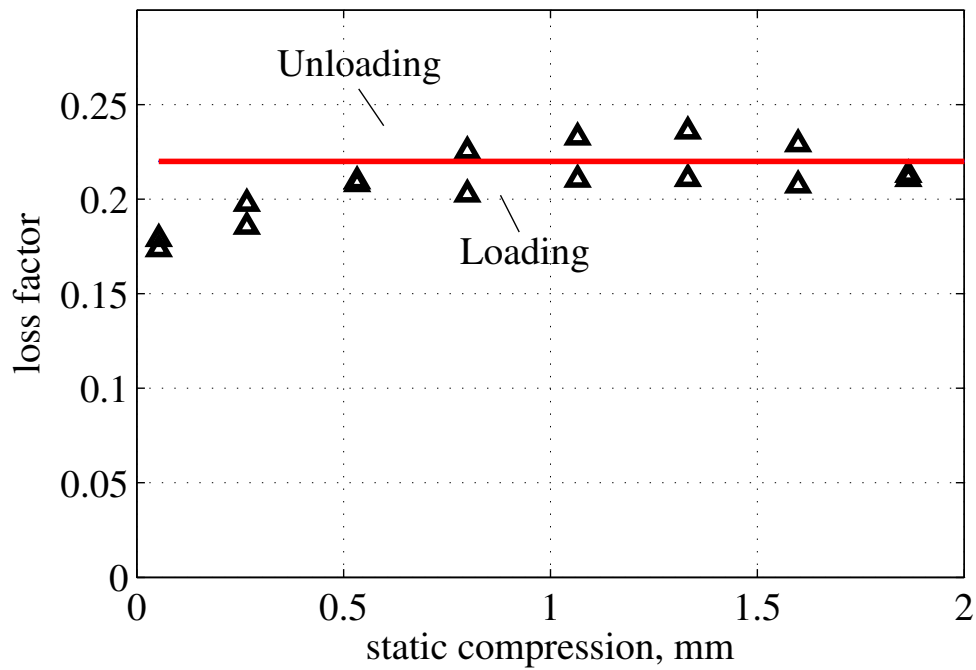

Figure 8: Analytical damping model for O-ring. red solid line refers to developed model. Black triangle refers to experimental data

4.2. Rocking behaviour

The rocking mode, in which the damper rotates about an axis perpendicular to the central threaded rod, is a key feature for this type of TMD. The stiffness, under this kind of deformation, depends on the centre of rotation. Because of the symmetrical nature of the damper, this occurs at the midpoint of the threaded rod. A simplified sketch is illustrated in Figure 9.
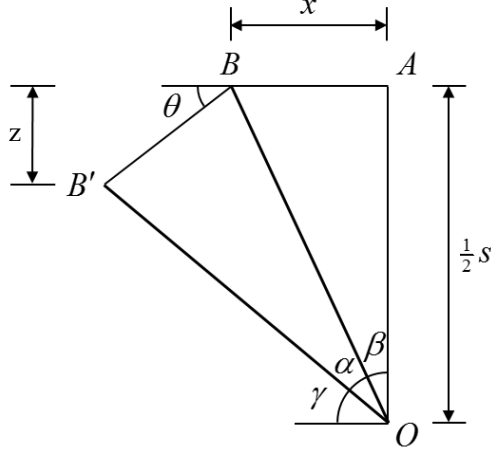

Figure 9: A schematic diagram of rocking mode. The O-ring has a nominal diameter of d_n and is centred around A. As the TMD rocks around an axis through O, the selected contact point moves from B to B'.

Note that α is the rotational angle of this TMD. z refers to the vertical deformation caused by rocking mode of this TMD. B is any selected point in the contact area of the deformed ring, and the distance between B and symmetric axis of the circular disc is defined as x. It is assumed that the length of threaded rod is s. The rotational axis goes through Point O. Using the geometric relationship shown in Figure 9, the vertical displacement caused by rotational motion can be expressed as,

$$z = \frac{s}{2} - \overline{OB'} \sin\left(\frac{\pi}{2} - \alpha - \beta\right) \tag{13}$$

Since the $\overline{OB}$ is equal to $\overline{OB'}$, Equation 13 can be rearranged using trigonometric identities:

$$z = \frac{s}{2}\left(1 - \cos\alpha\right) + x\sin\alpha \tag{14}$$

When the vibrational amplitude is small, the high order terms in this expression are negligible. Therefore, the vertical deformation at selected point B is

$$z = x\alpha \tag{15}$$

The rotational stiffness of this TMD is then formulated using equivalent strain energy. The underlying assumptions for this analysis are as stated below,

- The cross-section of the O-ring can be represented by an equivalent rectangle. This is a reasonable approximation if the O-ring is subjected to significant axial compression.

- As the dynamic amplitude is much less than the static compression, the compressive stiffness remains unchanged during vibration.

- The stiffness is uniform through the cross section of O-ring as the nominal diameter is much larger than the cross-sectional diameter.
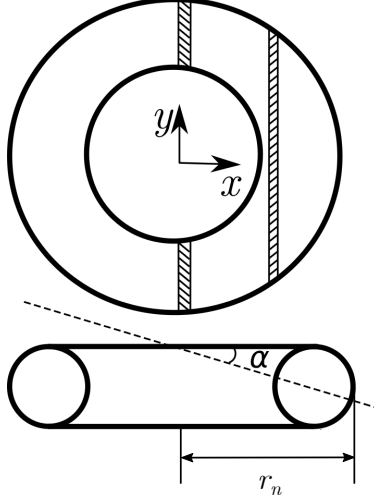
11

Figure 10: A schematic diagram of rocking modes

The coordinate for the subsequent analysis for rotational motion of this TMD is shown in Figure 10.

The overall cross-sectional area of O-rings change with different static compressions. Using the equivalence between practical deformed and assumed rectangular cross-sectional area, the average wire radius can be estimated in the width direction, as shown in Equation 16.

$$R_0^{\text{eq}} = \frac{8a + 8R}{3} \tag{16}$$

The equivalent outer and inner radius can be given by,

$$r_2 = r_n + R_0^{\text{eq}} \tag{17}$$

$$r_1 = r_n - R_0^{\text{eq}} \tag{18}$$

where r_n is the nominal radius of O-ring. The equivalence of strain energy between the rotational and translational coordinate can be given by,

$$
\frac{1}{2} k_{\text{rot}} \alpha^2 = 2 \int_0^{r_1} k' \left(2\sqrt{(r_2{}^2 - x^2)} - 2\sqrt{(r_1{}^2 - x^2)} \right) \frac{1}{2} z^2 dx \\
+ 2 \int_{r_1}^{r_2} 2k' \sqrt{(r_2{}^2 - x^2)} \frac{1}{2} z^2 dx
\tag{19}
$$

in which k' is average compressive stiffness per cross-section and x is the location along the cross section. Note that the relationship between rotational angle α and position x is defined in Equation 15. After rearrangement of Equation 19, the equivalent rocking stiffness can be expressed by,

$$k_{\text{rot}} = \frac{\pi}{4} k' \left(r_2{}^4 - r_1{}^4 \right) \tag{20}$$

Here, the average stiffness is represented as

$$k' = \frac{\lambda k_{\text{c}}}{\pi \left(r_2{}^2 - r_1{}^2 \right)} \tag{21}$$

where k_{c} is the compressive stiffness of the cross-sections at given compression and λ is the shape factor that accounts for the effect of curved edges on the load-carrying capability. For an elastomeric annulus,

12

Payne [21] provides the empirical expression for the shape function,

$$\lambda = 1.33 + 0.12 \left(\frac{r_2 - r_1}{2R - w} \right)^2 \tag{22}$$

where $2R - w$ is the effective thickness of O-ring.

Combining Equation 20 with 21, the rotational stiffness for the O-ring at selected static compression is represented as,

$$k_{\text{rot}} = \frac{1}{4} \left(r_1{}^2 + r_2{}^2 \right) \lambda k_c \tag{23}$$

For the analytic model developed here, some points need to be highlighted. The analytical rocking model is based on the compressive stiffness model, which assumed that the O-rings are simulated using a rectangular ring with the same cross-sectional area. The effect of the curved edges of the deformed cross-section is explained using the shape factor. Errors, especially those occurring when the O-ring is subjected to a rotational moment, are introduced because the movement of the centroid is not accounted for in the proposed model. In practice, the centroid of the cross-section shifts horizontally with static compression, thus stiffening the O-rings in the rotational direction. Also, the equation that estimates the contact length loses its effectiveness at high compressions, which stiffens the proposed analytical model.

5. Validation

This section reports work done where a validation rig was used to evaluate the effectiveness of the analytical models established in previous sections. One of the most important requirements of the rig was that the moving parts needed to have similar rigid body motion behaviour to that of the proposed TMD.

5.1. Test configurations

The details of the experimental apparatus are shown in Figure 11.

This validation rig used two fixed masses that were mechanically attached to a threaded rod. A centre moving mass was placed between these two fixed discs. Two O-rings were then located between the moving and fixed masses. The selected static compressions were accomplished by rotating threaded rod. Slip gauges were used to ensure the accuracy of the static compression of the O-rings. Note that the two O-rings were assumed identical - thus achieving similar static compression. The properties of this validation rig are shown in Table 4.

Table 4: Properties of validation rigs

Variable	Value
Mass of the moving disc	441.52 g
Mass Moment of Inertia of the moving disc	$1.02 \times 10^{-4} \text{m}^4$
Dimensions of the moving disc	$\varnothing 50$ mm $\times$ 30 mm
Type of O-ring	Nitrile BS312

Excitation from a random source, limited by an analogue filter to the range 50 to 1000 Hz, was applied by mounting this device on a shaker capable of 489 N peak sine force via a piezoelectric force transducer. Two miniature accelerometers were mounted on the top and moving discs to measure the relative displacement of fixed and moving mass. For each test, a total collection time was 3.2 s at a sampling rate of 2560 Hz was selected. The ensemble average of frequency spectra over 20 cycles was used to remove noise. The base excitation captured by the accelerometer on the top mass is transferred to the rigid moving mass. Two different static compressions for the O-rings were chosen and the results, presented as transmissibility between the fixed and moving mass, are obtained. For each transmissibility curve, at least two resonances exist for both static compression under 700 Hz. The Nyquist circles of these transmissibilities were used to identify the resonance frequencies and corresponding damping accurately.
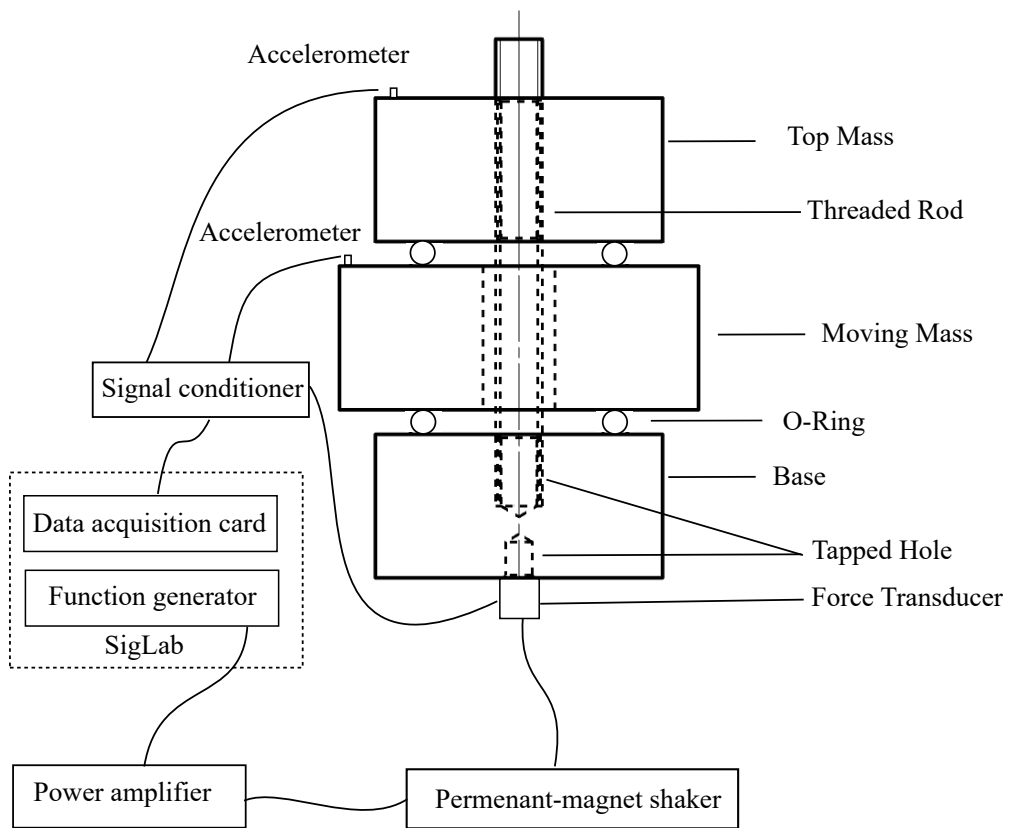
Figure 11: Sketch of test-rig for validation of stiffness in different modes

5.2. Compararive studies

A comparative prediction of the natural frequencies was conducted using the semi-empirical model developed. Despite being far from the glass transition, slight frequency dependence did exist and had to be accounted for. The frequency dependent modulus for the nitrile rubber used [22] could be represented by the following expression over the range of interest:

$$\log_{10} E = 0.094 \log_{10} \omega_n + 7.03 \tag{24}$$

As the natural frequencies changed with modulus, a few iterations were required to obtain final values. Multipliers of 1.53 and 1.66 were applied to the elastic modulus of nitrile rubber for a static compression of 0.3 and 1.9 mm, respectively. Calculated stiffness values of the analytical model are shown in Table 5.

Table 5: Analytical parameters of validation rigs

Static compressions	Stiffness	Values
0.3 mm	compressive	547.7 N/mm
	rotational	40.4 Nm/rad
1.9 mm	compressive	2687.5 N/mm
	rotational	209.1 Nm/rad

When the damping is relatively small, the damping ratio of the system can be given by [15]

$$\zeta = \frac{\eta}{2} \tag{25}$$

where η is energy loss factor of the O-ring. Comparisons of the theoretical prediction and experimental results are shown in Figure 12.
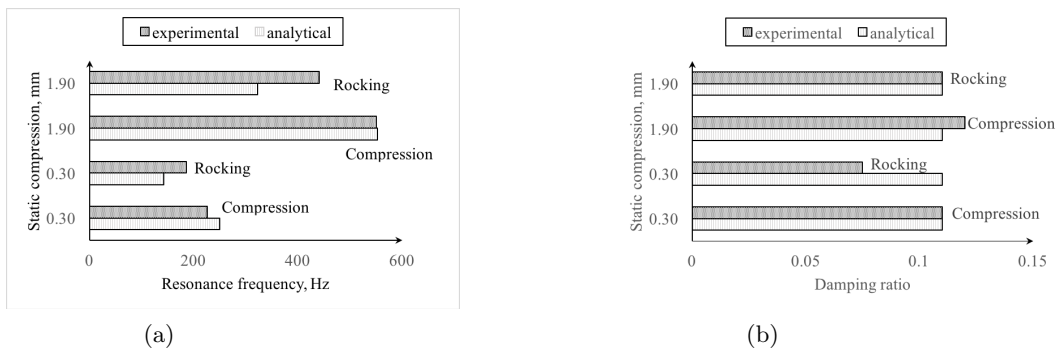

Figure 12: Comparisons of modal properties between analytical models and experimental results (a) resonance frequencies (b) damping

In Figure 12(a), it can be seen that the measured stiffness compares well with theoretical predictions for compression behaviour. For rocking modes, the resonance frequencies obtained from experiments are higher than those from the analytical model. One possible reason is misalignment of the O-rings during assembly as eccentricity can stiffen the TMD by moving material further from the rotation axis. The prediction accuracy for damping is generally very good, indicating (as expected) that the main damping mechanism is deformation within the O-ring material. The exception occurs for the rocking mode at low compression where the measured damping level is somewhat lower than predicted and is also lower than that for the other modes. The cause of this is uncertain but could again be attributed to misalignment.

6. Case study

Results from the previous section suggest that this type of TMD can work over a wide range of frequencies. This section presents the performance of this adjustable TMD when it was applied to a test structure in the form of a hollow aluminium beam. The acceleration frequency response function was obtained to evaluate whether this type of TMD could alter the target modes of the host structure.

6.1. Test procedure

The test set-up is presented in Figure 13. The adjustable TMD was attached to a box-section beam mounted on low-loss rubber supports at each end. The rubber blocks provides a repeatable boundary condition that also reduced vibration transmission between the ground and the structure. The overall length of the beam was 500 mm. In order to avoid the nodes for target modes, loading was applied at a position 115 mm from one end of the beam and the accelerometer was attached 385 mm from the same end. Two displacement laser probes were placed on both sides of the beam to measure the pre-strain on the O-rings. Because O-rings exhibit high nonlinear stiffness, identical static deformations were required for the O-rings on both sides.
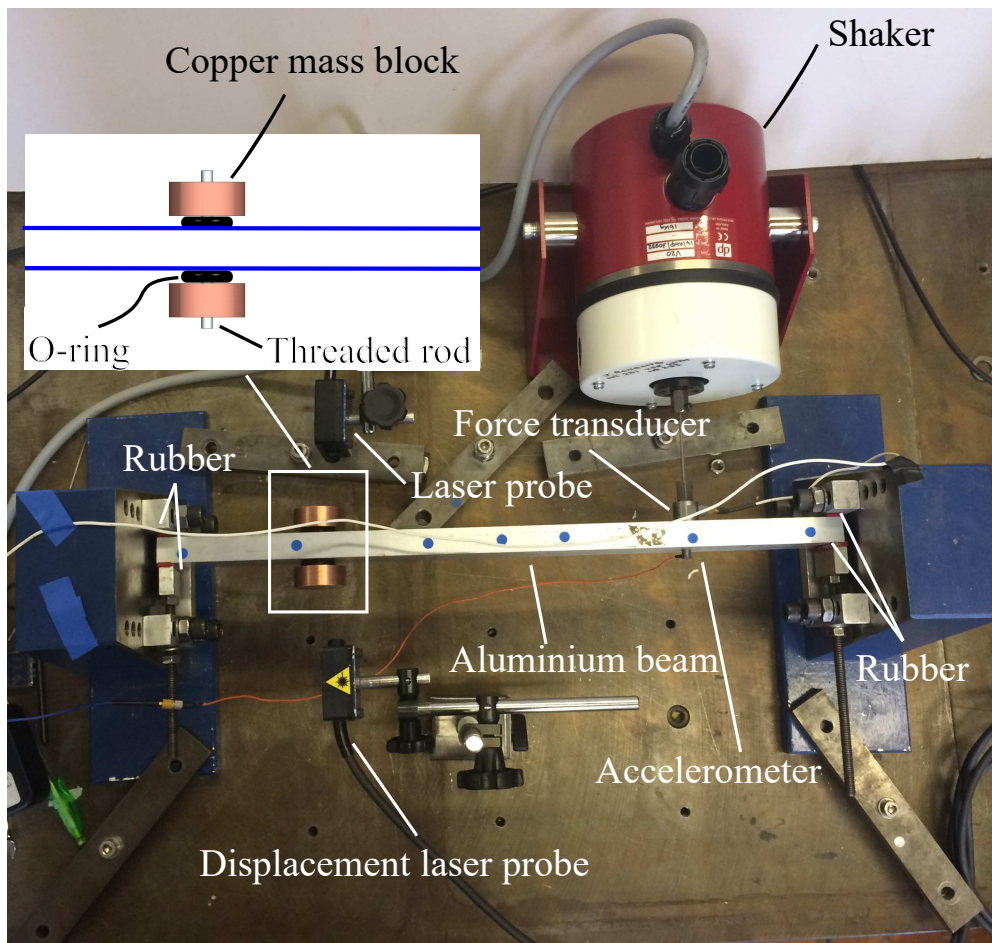

Figure 13: Test-rig for the rubber-end hollow beam

The detailed mechanical properties of the host structure are listed in Table 6.

It has been shown in the previous study that very little nonlinearity is present in this host structure [22]. Compared with energy dissipation from the TMD, the damping from the isolation rubber can be ignored.

16

6.2. Choice of the TMDs' parameters

The proposed TMD has two working modes in the selected frequency range of the host structure. In practice, the design parameters of the O-ring TMD can be optimised using both the tension-compression and rocking modes. When employing suitable design parameters of the TMD, this TMD can achieve the best performance of vibration suppression over wide frequency ranges. In this preliminary analysis however, only the motion of the TMD in compression-extension were selected as the targeted working modes.

In order to design the optimal TMD, the size of the attached discs need to be determined first. The diameter of the disc selected here is close to the width of the beam to widen the selections of O-rings. The choice of the thickness is based on the following requirements:

- resonances of the discs in vertical directions should not affect the working modes of the TMD;

- discs should apply uniform static strain on the O-rings using simple threaded connections;

- mass of discs should ensure the correct working frequencies of the TMD.

In this example, the two copper discs and threaded rod have a mass of approximately 320g. Once the masses of the discs were determined, the design parameters of circular O-rings were then selected. Nitrile O-rings with circular cross sections were used due to their low cost and suitable damping. Since typical elastomeric TMDs suffer from their high resonance frequencies, relative soft O-rings with large cross-sectional diameter were considered suitable. Regarding the geometric limitations of the host structure, BS312 O-rings were selected in this example. The detailed dimensions of the TMD can be reviewed in Table 1. Following this, a pre-strain - resonance frequencies master curve was established for this TMD, as shown in Figure 14.

Table 6: Mechanical properties of host structure

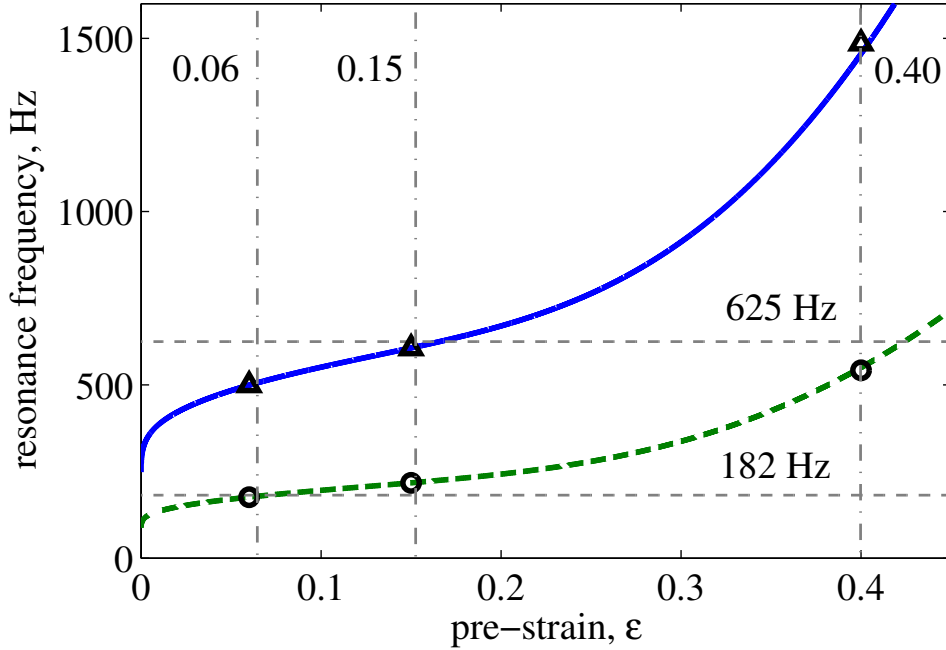| Components	Variable	Unit	Value
Hollow beam	Elastic modulus	GPa	69
	Dimensions	mm	$500 \times 38.1 \times 19.1$
	Wall thickness	mm	2.5
	Mass	g	290 g
Isolation rubber	Elastic modulus	MPa	8.3
	Dimensions	mm	$19.1 \times 10 \times 3$
	Loss factor	-	0.08 - 0.1

Figure 14: Resonance frequencies of the TMD when subjected to various pre-strains (blue solid line: resonance frequency for compression mode; green dash-dot line: resonance frequency for the rocking mode; red dot line: natural frequency of 1st structural mode; cyan dot line: natural frequency of 2nd structural mode

For the host structure, the first two resonance frequencies are approximately 182 and 625 Hz. If the host structure has little damping, it has been shown [1, 23] that the optimal performance can be obtained when the resonance frequency of the TMD is close to that of the host structure. In Figure 14, it can be seen that interactions between structural and damper modes occur when the pre-compression is approximately 6%, 15% and 40% of the wire diameter. For the relatively small O-ring used in this work, 6% compression was considered to be near the lower limit in terms of what could be applied reliably. Under this compression level, the TMD rocking mode targets the first mode of the structure. When the pre-compression is increased to 15%, the tension-compression mode also targets the second structural mode. Finally, at 40% compression, the rocking mode of the TMD approaches the second mode of the structure.

6.3. Performance of the TMD at selected pre-strains

Figure 15 and 16 show the acceleration frequency responses for the host structure with the TMD subjected to different working conditions. When the O-ring was subjected to a static compression of 6%, lateral vibrations at the first structural resonance (around 185 Hz) were suppressed by a factor of 10. As pre-compression was increased, damping of the first mode became less effective. At a pre-compression of 40%, the vibration level near 600 Hz (associated with the second structural mode) was almost 8 times lower. Finally, at 15% compression, the condition indicated in Figure 14 as optimal in terms of addressing both structural resonances, it can be seen that both resonances are suppressed effectively. These results confirm what was expected from the predictive work and demonstrate that effectiveness of the design approach used.
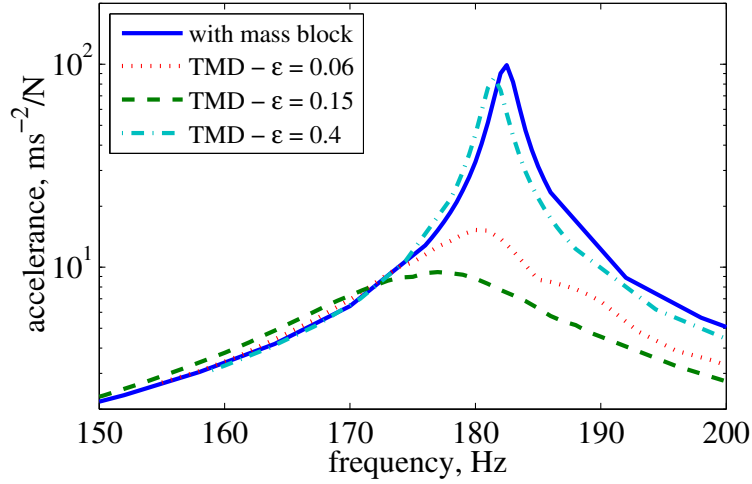
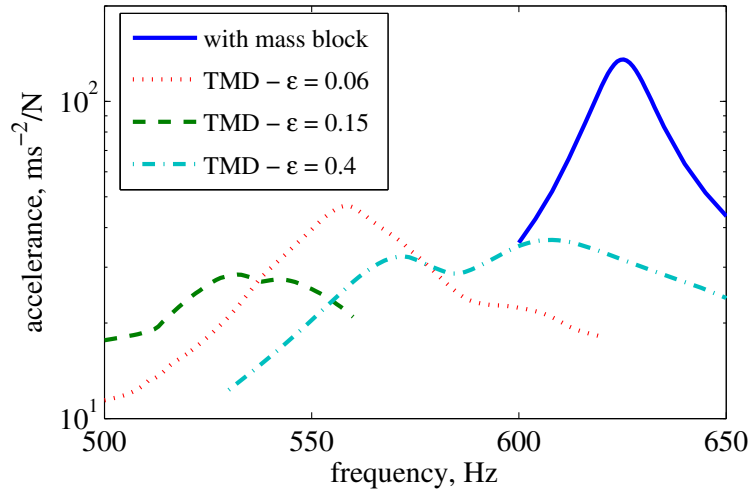Figure 15: Performance of O-ring TMD with various pre-strains for the 1st mode

Figure 16: Performance of O-ring TMD with various pre-strains for the 2nd mode

7. Design considerations for practical applications

The case study conducted in Section 6 shows how initial sizing calculations can be performed adequately for an adjustable O-ring based TMD. A complete design evaluation should consider performance over its lifetime under different environmental conditions. While such a detailed activity lies outside the scope of this paper, the nature of the O-ring does raise particular challenges that are briefly identified here.

The operating environment defines the suitability of a particular O-ring material. Depending on the application, adequate precautions must be taken to avoid degradation from exposure to different types of radiation, outgassing and chemical attack. All polymers have a maximum temperature above which physical degradation occurs and a minimum below which the material becomes too brittle to be of practical use. The range over which the material can safely be used, depends on the material selected: for the nitrile rubber O-rings used in this study, this range is -40 to 100 ºC. To minimise frequency and temperature dependence, material selection in this work involved aligning the rubbery zone of the elastomer with the

19

operating conditions. While design for operation near glass transition is theoretically possible through the use of the complex modulus from the viscoelastic master curve, its high sensitivity to frequency and temperature around transition makes working in this zone less attractive as significant detuning could be caused by a relatively small temperature excursion. For nitrile O-rings, setting the lower temperature limit to 0 °C would avoid these problems.

Although elastomer O-rings are made from cross-linked polymers with a defined rubbery plateau, it is likely that some changes over time will arise from the steady load associated with the pre-compression. In the design studied here, the deformation is controlled by the threaded rod. Hence over time, relaxation within the material could occur resulting in a small reduction of modulus. However, because it is the deformation rather than the load that is controlled, the geometry will not change significantly and so the overall effect on the system stiffness, and therefore the effect on the tuning of the TMD, will be relatively small.

Physically, the construction of the damper is extremely simple. When assembling the damper on the host structure, care needs to be taken to align the centre of the O-ring with the centre of the tensioning rod differences between these can affect the natural frequency of the rocking mode. If features are added to simplify accurate location, for example, a shallow groove in each disc forming the moving mass, they may change the contact condition and the overall stiffness. However, if the feature is shallow in comparison to the level of compression, the frequency change will also be small in comparison with effects already noted such as interface slip and amplitude-dependent softening (Payne effect).

8. Conclusions

A novel TMD configuration has been proposed that is based on elastomeric O-rings. Analytical models and physical experiments have been used to reach the conclusions outlined below.

1. The geometrical nonlinearity of the O-rings allows adjustment of the TMD stiffness, enabling simple in-situ tuning of the device.
2. Analytical and semi-empirical formulae can be used to size the O-ring, and the TMD, for a given practical application.
3. Off-axis vibrations that link with the rocking mode of the TMD need to be considered as they can influence the motion of the host structure, and therefore can be used in the overall vibration control strategy.
4. The O-ring TMD can be adjusted to operate over a wide range of frequencies and can simultaneously target more than one structural resonance.

The proposed device was a through-bolted configuration that needs access to both sides of the flexible host structure. However, it would be straightforward to extend the approach to include configurations that do not require this design constraint.

References

[1] J. Den Hartog, J. Ormondroyd, Theory of the dynamic vibration absorber, Journal of Applied Mechanics 50 (1928) 11–22.
[2] L. Zuo, S. Nayfeh, Minimax optimization of multi-degree-of-freedom tuned-mass dampers, Journal of Sound and Vibration 272 (2004) 893–908.
[3] M. De Angelis, S. Perno, A. Reggio, Dynamic response and optimal design of structures with large mass ratio TMD, Earthquake Engineering & Structural Dynamics 41 (2012) 41–60.
[4] I. Lazar, S. Neild, D. Wagg, Vibration suppression of cables using tuned inerter dampers, Engineering Structures 122 (2016) 62–71.
[5] D. Pietrosanti, M. De Angelis, M. Basili, Optimal design and performance evaluation of systems with Tuned Mass Damper Inerter (TMDI), Earthquake Engineering & Structural Dynamics 46 (2017) 1367–1388.
[6] A. Reggio, M. De Angelis, Optimal energy-based seismic design of non-conventional tuned mass damper (TMD) implemented via inter-story isolation, Earthquake Engineering & Structural Dynamics 44 (2016) 1623–1642.
[7] M. Acar, C. Yilmaz, Design of an adaptive–passive dynamic vibration absorber composed of a string–mass system equipped with negative stiffness tension adjusting mechanism, Journal of Sound and Vibration 332 (2013) 231–245.
[8] S. Nagarajaiah, Structural vibration damper with continuously variable stiffness, 2000. US Patent 6,098,969.
[9] Y. Yang, D. Xu, Q. Liu, Milling vibration attenuation by eddy current damping, The International Journal of Advanced Manufacturing Technology 81 (2015) 445–454.

[10] D. Pisarski, C. Bajer, B. Dyniewicz, J. Bajkowski, Vibration control in smart coupled beams subjected to pulse excitations, Journal of Sound and Vibration 380 (2016) 37–50.

[11] A. Hassan, A. Torres-Perez, S. Kaczmarczyk, P. Picton, Vibration control of a stirling engine with an electromagnetic active tuned mass damper, Control Engineering Practice 51 (2016) 108–120.

[12] S. Sun, J. Yang, W. Li, H. Deng, H. Du, G. Alici, T. Yan, An innovative MRE absorber with double natural frequencies for wide frequency bandwidth vibration absorption, Smart Materials and Structures 25 (2016) 35–55.

[13] J. Ferry, Viscoelastic properties of polymers, John Wiley & Sons, 1980.

[14] P. Lindley, Compression characteristics of laterally-unrestrained rubber O-rings, Journal of the Institution of the Rubber Industry 1 (1967) 209–213.

[15] D. Mead, Passive vibration control, John Wiley & Sons Inc, 1999.

[16] J. Diani, B. Fayolle, P. Gilormini, A review on the Mullins effect, European Polymer Journal 45 (2009) 601–612.

[17] A. Payne, The dynamic properties of carbon black-loaded natural rubber vulcanizates. Part i, Journal of Applied Polymer Science 6 (1962) 57–63.

[18] A. Gent, P. Lindley, The compression of bonded rubber blocks, Proceedings of the Institution of Mechanical Engineers 173 (1959) 111–122.

[19] A. George, A. Strozzi, J. Rich, Stress fields in a compressed unconstrained elastomeric O-ring seal and a comparison of computer predictions and experimental results, Tribology International 20 (1987) 237–247.

[20] K. Johnson, Contact Mechanics, Cambridge University Press, 1985.

[21] A. Payne, J. Scott, Engineering design with rubber, Maclaren et Sons, 1960.

[22] N. Tang, N. Sims, J. Rongong, Modelling of an adjustable TMD incorporating an elastomeric O-ring, in: Proceedings of 17th International Conference on Experimental Mechanics, Rhodes, 2016.

[23] J. Brock, A note on the damped vibration absorber, Journal of Applied Mechanics (1946).